CrystEngComm

ROYAL SOCIETY OF CHEMISTRY

PAPER

View Article Online
View Journal | View Issue

Cite this: *CrystEngComm*, 2024, **26**, 6161

Some aspects of MOF-74 (Zn_2DOBDC) metal–organic framework formation using THF as the solvent†

Alena A. Starodubtseva,[a] Vladislav A. Dubrovskiy,[b] Seiilbek D. Malik,[a] Konstantin A. Lyssenko,[d] Aliya M. Sembayeva,[e] Aleksandr A. Morontsev,[f] Alina K. Galeyeva[a] and Ivan A. Trussov *[ac]

This study investigates the synthesis of zinc-based metal–organic frameworks (MOFs) using tetrahydrofuran (THF) as a solvent, focusing on forming distinct phases as models for potential battery applications. Contrary to expectations, the synthesis produced three unique phases: alpha, beta, and Zn-MOF-74a, instead of the anticipated Zn-MOF-74 structure. Comprehensive structural analysis using X-ray diffraction, infrared spectroscopy, and thermogravimetric analysis (TGA) revealed distinct crystallographic features for each phase, particularly the novel Zn-MOF-74a phase, which exhibits a heart-shaped pore structure and differs from the classic hexagonal MOF-74. The study also includes the first structural determination of the dry H_4DOBDC precursor, providing crucial insights for future research. The results demonstrate the significant impact of solvent choice, temperature, and pH on MOF phase formation and offer potential applications in energy storage and catalysis, especially for larger molecules. Further investigation is required to fully understand the electrochemical properties and phase stability of the newly identified Zn-MOF-74a and beta phases.

Received 8th September 2024,
Accepted 16th October 2024

DOI: 10.1039/d4ce00905c

rsc.li/crystengcomm

1. Introduction

Studying metal–organic frameworks (MOFs) for battery applications is crucial due to their improved energy storage capabilities, efficient ion transport, and reversible ion insertion/extraction originating from their high surface area, tunable properties, and porosity. Additionally, MOFs offer multifunctionality and the potential for integrated energy storage systems, leading to advancements in renewable energy storage, electric vehicles, and portable electronics.[1–3] MOFs encounter particular challenges, particularly concerning stability and conductivity in batteries.[4,5] This is because most microporous MOFs are electrical insulators. Recent developments in this field show that careful selection of metal and organic counterparts can result in crystalline porous materials with highly favorable conductivity and charge mobility properties.[6–8]

Among the various MOFs, MOF-74 (M–DOBDC, where M = Mg, Mn, Fe, Co, Ni, Zn; DOBDC = 2,5-dioxide-1,4-benzenedicarboxylate) has shown promise due to its catalytic activity[9,10] and gas adsorption properties,[11–13] which suggests that it has potential as an electrode material.

However, the high sensitivity of transition metal-based MOF-74 to oxidizing conditions necessitates the search for more stable alternatives. In this context, zinc-based MOF-74 is particularly noteworthy as a model compound for studying such materials' electrochemical behavior and stability due to its simple synthesis, environmental friendliness, and low cost.[14–16]

There are many ways to synthesize Zn-based MOF-74 characterized by differences in the number of steps required, stoichiometric ratios, reaction time, temperature conditions, choice of solvent, and other factors.[17–21] A commonly used method for synthesizing Zn-based MOF-74 is solvothermal synthesis, which involves using dimethylformamide (DMF)–water mixture as the solvent.[22] Another known synthesis method for MOF-74 is the co-precipitation method at room temperature using methanol as the solvent.[23] It is essential

[a] *Center of Phisico-Chemical Methods of Research and Analysis, Al-Farabi Kazakh National University, Almaty, 010000, Kazakhstan*
[b] *Scientific Research Institute of New Chemical Technologies and Materials, Al-Farabi Kazakh National University, Almaty, 010000, Kazakhstan*
[c] *Skoltech Center for Electrochemical Energy Storage, Skolkovo Institute of Science and Technology, Moscow, 121205, Russian Federation.*
E-mail: ivan.trussov@hotmail.com
[d] *M. V. Lomonosov Moscow State University, Moscow, 119991, Russia*
[e] *Science Fund JSC, Astana, 010000, Kazakhstan*
[f] *A. V. Topchiev Institute of Petrochemical Synthesis, RAS Russia, Moscow, 119991, Russia*

† Electronic supplementary information (ESI) available. CCDC 2382749 and 2382750. For ESI and crystallographic data in CIF or other electronic format see DOI: https://doi.org/10.1039/d4ce00905c

to note that DMF or methanol tends to adsorb within the MOF-74 pores, posing challenges for complete solvent removal even after thorough washing.[24]

The filling and diameter of channels within the MOF-74 structure should play a crucial role in its ion transport properties. During the synthesis process, specific solvent molecules (*i.e.*, DMF or methanol) can become trapped within the pores due to the formation of solvate-cation solid bonds, hindering pore evacuation. However, using a less polar solvent alternative could affect the filling of these pores. One alternative solvent is tetrahydrofuran (THF), which has lesser polarity than DMF or methanol. By switching to THF, the filling of pores in MOF-74 may be influenced by differences in the size and interactions of THF molecules with the material's pore structure. Dietzel *et al.* conducted a study that synthesized a nickel-based MOF-74 through the solvothermal method using a tetrahydrofuran (THF)–water mixture as the solvent.[25] Using THF potentially leads to more efficient channel evacuation, given that its removal from the channels is facilitated, allowing for swifter ion migration through the network.

In this study, we set out to synthesize Zn–DOBDC-based MOF-74 using THF as the solvent. Contrary to our expectations, this modification in the solvent system led to the formation of different distinct metal–organic phases rather than the anticipated MOF-74 structure. We conducted a thorough structural analysis of these phases, identifying them as alpha, beta, and Zn-MOF-74a phases with distinct crystallographic characteristics. Additionally, we successfully determined the structure of the dry precursor H_4DOBDC, for which there appears to be no existing data in the literature.

2. Experimental

Synthesis of Zn-MOF-74a

0.439 g (2 mmol) of zinc acetate dihydrate ($Zn(CH_3COOH)_2{\cdot}2H_2O$, Sigma-Aldrich, 98%) and 0.198 g (1 mmol) of 2,5-dihydroxyterephthalic acid (H_4DOBDC, Sigma-Aldrich, 98%) are dissolved in 19.6 mL of tetrahydrofuran (THF, Honeywell, 99.9%). The resulting mixture is thoroughly mixed and placed in an autoclave with a 50 mL glass liner (Innovaster). The autoclave is kept at a temperature (140–180 °C) for 60 hours. The resulting crystals are separated by centrifugation from the mother liquor and washed three times with distilled water and three times with ethanol. They are then dried under a vacuum at 110 °C for 12 hours.

Synthesis of alpha and beta phases

A solution of 0.439 g (2 mmol) of zinc acetate dihydrate $Zn(CH_3COOH)_2{\cdot}2H_2O$ (Sigma-Algrich, 98%) in 13.5 ml of distilled water and a solution of 0.198 g (1 mmol) of 2,5-dihydroxyterephthalic acid (H_4DOBDC) (Sigma-Algrich, 98%) in 6 ml of tetrahydrofuran (THF, Honeywell, 99.9%) are mixed and placed in an autoclave with glass liner (Innovaster, 50 ml). The autoclave is kept at a temperature (23–180 °C) for 60 hours. The resulting crystals are separated by centrifugation from the mother liquor and washed three times with distilled water and three times with ethanol. They are then dried under a vacuum at 110 °C for 12 hours.

A powder X-ray diffraction analysis (XRD) was conducted on obtained samples using a MiniFlex Benchtop powder XRD diffractometer by Rigaku, equipped with a copper X-ray source ($\lambda_{CuK\alpha1}$ = 1.54056 Å, $\lambda_{CuK\alpha2}$ = 1.54439 Å).

The single crystals of Zn_2DOBDC·1.5H_2O, Zn$DOBDC(H_2O)_2$ and $Zn_{2.5}$DOBDC were selected from the powdered sample and mounted onto a Bruker D8 Quest with a Photon III detector diffractometer. The crystal was maintained at a temperature of 100.0 K while collecting data. The Bruker software package SAINT (version 8.40B)[19] was utilized for data reduction and integration. The data underwent corrections for both Lorentz and polarization effects to ensure accuracy. Due to the crystals' anisotropic shape and strong absorption of X-ray radiation, absorption correction was carried out using a numerical approach and a multiscan routine using SADABS (version 2016/2).[20] The structure was solved using Olex2[21] and the ShelXT[22] program for structure solution through intrinsic phasing. It was then refined using the ShelXL[23] refinement package and least squares minimization. Structure refinement by the Rietveld method was carried out using the TOPAS software package with the TOPAS-Academic script library.[26]

Infrared spectroscopy (FTIR) was used to study the structure and identify the specifics of the samples. IR spectra were recorded using a Bruker HYPERION 2000 FTIR microscope and an IFS-66 v/s Fourier spectrometer. The recording was performed on a ZnSe crystal range from 600 to 4000 cm^{-1} with a 2 cm^{-1} resolution.

The TGA analysis was performed utilizing an F3 STA-449 apparatus (Netzsch, Germany) combined with a mass spectrometer QMS 403 D Aeolos (Netzsch, Germany) in an oxygen–argon atmosphere with heating at a rate of 5 °C min^{-1} to 800 °C.

3. Results and discussion

We investigated the synthesis of MOF-74 using a solvothermal route to prevent potential solvent (in this study, we used in-methanol-prepared MOF-74 for comparison; it was prepared following procedure by Flores *et al.*[23]) build-up in the pores. To achieve this, we produced a range of samples at different temperatures (23–210 °C). Based on the stoichiometric ratio, the average yield of a solid product was over 80% of the theoretical.

To analyze the formation patterns of the samples, we conducted a comparison of XRD diffractograms. For a better visual comparison of the diffraction data (Fig. 1), we relied on the logarithm of the signal intensity due to the synthesized samples being greatly influenced by texturing. The XRD analysis showed that the diffraction patterns obtained do not match the expected structure of MOF-74. Instead, we identified two distinct diffraction patterns that originated from two phases, namely alpha and beta. It has been conclusively determined that a first single phase (alpha) is consistently present when temperatures remain below 110

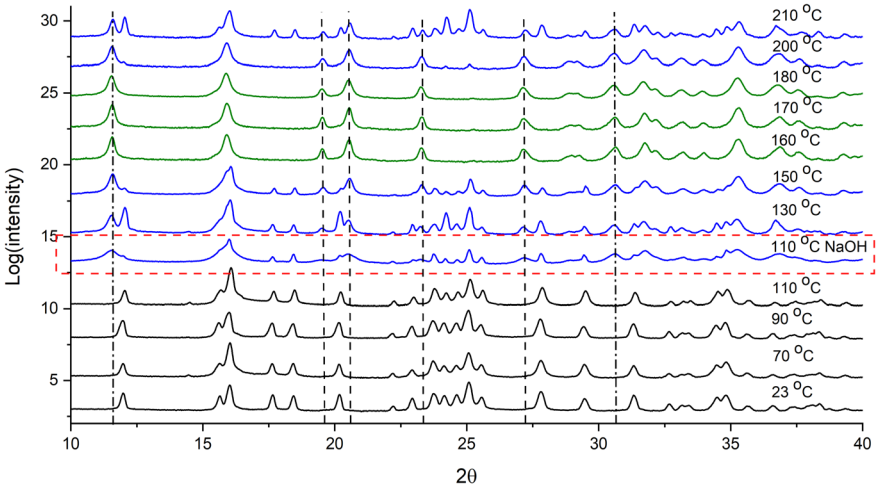

Fig. 1 X-ray diffraction patterns of samples obtained at various temperatures and pH solvothermal synthesis in THF/H_2O. Black is pure alpha; green is pure beta; red is a mixture of alpha and beta. The dashed rectangle designates the sample obtained *via* Nijem *et al.* route.[27]

°C (white crystalline powder). However, a mixture of two phases (alpha and beta) can be observed between 130 °C and 150 °C. In the temperature range of 160 °C to 180 °C, a single-phase structure (beta) reappears (reddish-orange crystalline powder). With an increase in temperature to 200 °C and above, the appearance of an impurity alpha phase is observed again. No pronounced amorphous halo indicates the absence of significant amounts of amorphous impurities.

Previously, Nijem *et al.* claimed the synthesis of MOF-74 using THF as a solvent; however, they also added NaOH.[27] Their method differs from ours in the ratio of the solvents (THF–H_2O–NaOH 7 : 3 : 2 *vs.* THF–H_2O 6 : 13.5). One of the critical points for us was the assumption about the possible effect of higher pH on the formation of the MOF-74 phase. The lowering of pH was presumed to keep DOBDC molecules only partially protonated and decrease the ability to coordinate into a metalorganic framework. To test this hypothesis, we repeated the synthesis as described by Nijem *et al.*[27] During this procedure, when mixing the initial reagents in a mixture of THF–H_2O solvents, we observed a pH of 3.5, which can probably explain the deprotonation of dihydroxobenzene dicarboxylic acid. When NaOH was added, the pH shifted to the neutral region, reaching a value of 6.5. The entire synthesis process was carried out at 110 °C for 72 hours. The final product was in the form of a yellow powder. However, the XRD results did not match the expected structure of MOF-74 described in a previous study by Nijem *et al.* (Fig. 1 – rectangular selection). Instead, we identified a mixture of alpha and beta phases, similar to our earlier findings. Interestingly, when using THF–H_2O solvents in a ratio of 6 ml : 13.5 ml at a temperature of 110 °C, peaks characteristic only of the alpha phase were seen in the diffraction pattern. Additionally, to study the effect of pH on the process of phase formation, an additional synthesis was carried out according to Nijem *et al.* but without NaOH. In this case, we used a mixture of solvents THF–H_2O in a 7 ml : 3 ml ratio at a pH of about 3.5. However, as a result of this experiment, only an amorphous halo was observed in the diffraction pattern, indicating the formation of an amorphous product.

The swift investigation of the experimental section of the Nijem *et al.* study[27] showed that they followed the procedure by Zhou *et al.*[28] Further, Zhou *et al.* mention that they followed the procedure by Rosi *et al.*[29] Interestingly, in the latter study, they report the DMF route instead of THF for Zn-based MOF-74. We suspect an upsetting typo in the description of the experimental section in the Nijem study[27] since we found no evidence of the Zn-based MOF-74 formation using THF either *via* original or modified procedures.

In our continued investigation, we hypothesized that competitive coordination of water molecules with zinc ions might inhibit the formation of MOF-74. Water's high polarity and strong affinity for zinc ions can interfere with the coordination between zinc ions and organic ligands, thus preventing the formation of the desired crystal structure. To test this hypothesis, we sought to minimize the water content in the reaction mixture by using absolute THF as the solvent, with the only remaining water originating from the crystallohydrate precursor.

The results of this experiment are presented in Fig. 2, which reveals the emergence of a new phase at temperatures ranging from 140 °C to 160 °C. This phase does not correspond to the alpha or beta phases or the expected MOF-74 structure. However, the overall diffraction pattern bears a resemblance to MOF-74. We have designated this new phase as Zn-MOF-74a. The data suggest that Zn-MOF-74a becomes the predominant phase as the temperature increases. Below 170 °C, the samples contain unknown impurities, but above this temperature, a pure phase of Zn-MOF-74a is obtained, appearing as a yellow crystalline powder.

To further investigate the samples' structure, we attempted to obtain single crystals for diffraction analysis. Single crystals of the alpha phase were successfully extracted from the powdered sample, while the beta phase presented

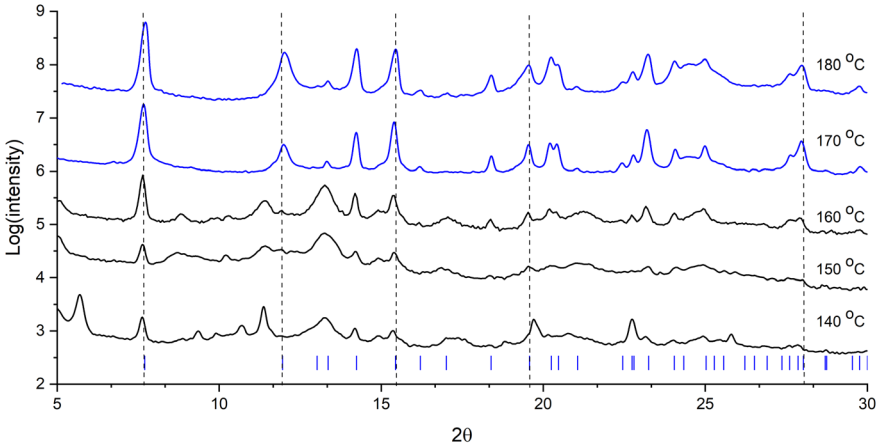

Fig. 2 X-ray diffraction patterns of samples obtained at various temperatures solvothermal synthesis in THF. Black is a mixture of phases; blue is pure Zn-MOF-74a.

challenges; despite various efforts, we could not grow or isolate single crystals for it, limiting our analysis to indexing its powder diffraction pattern. For Zn-MOF-74a, single crystals were successfully formed in absolute THF during regular synthesis. The summary of the single-crystal diffraction studies for the alpha phase and Zn-MOF-74a is presented in Table 1.

The analysis confirmed that the alpha phase, identified as monoclinic ($C2/c$) ZnDOBDC$(H_2O)_2$, aligns with the structure reported by Ghermani *et al.* and obtained by different synthesis root in much more alkali pH due to the addition of NaOH.[30] Due to the lack of novelty in the re-determination of this phase, the complete structural description of ZnDOBDC$(H_2O)_2$ was placed into supplementary. We

Table 1 Single crystal study information

Identification	ZnDOBDC$(H_2O)_2$ (alpha)	Zn_2DOBDC·1.5H_2O
Empirical formula	$C_8H_8O_8Zn$	$C_8H_2O_8Zn_2$·1.5H_2O
Formula weight	297.51	351.86
Temperature/K	100.0	295.00(10)
Crystal system	Monoclinic	Trigonal
Space group	$C2/c$	$R3c$
a/Å	15.451(3); 15.706(1) [RT a]	22.9353(4)
b/Å	5.2329(7); 5.330(1) [RT a]	22.9353(4)
c/Å	12.2017(16); 12.070(1) [RT a]	15.9392(3)
α/°	90	90
β/°	111.585(5); 110.651(1) [RT a]	90
γ/°	90	120
Volume/Å^3	917.4(2); 945.60(7) [RT a]	7261.2(3)
Z	4	18
ρ_{calc} g cm^{-3}	2.154	1.448
μ/mm^{-1}	2.711	2.989
F(000)	600.0	3114.0
Crystal size/mm^3	0.234 × 0.21 × 0.18	0.13 × 0.02 × 0.01
Radiation	MoKα (λ = 0.71073 Å)	MoKα (λ = 0.71073 Å)
2Θ range for data collection/°	5.67 to 59.116	3.552 to 52.716
Index ranges	$-21 \le h \le 21$	$-28 \le h \le 28$
	$-7 \le k \le 5$	$-28 \le k \le 28$
	$-13 \le l \le 16$	$-19 \le l \le 19$
Reflections collected	3517	169 979
Independent reflections	1290 [R_{int} = 0.1318, R_{sigma} = 0.1897]	3296 [R_{int} = 0.1554, R_{sigma} = 0.0261]
Data/restraints/parameters	1290/0/80	3296/8/108
Goodness-of-fit on F^2	0.855	1.089
Final R indexes [$I \ge 2\sigma(I)$]	R_1 = 0.0644, wR_2 = 0.1006	R_1 = 0.0724, wR_2 = 0.1925
Final R indexes [all data]	R_1 = 0.1032, wR_2 = 0.1155	R_1 = 0.0763, wR_2 = 0.1974
Largest diff. Peak/hole/e Å^{-3}	0.79/−1.09	2.76/−0.90
CCDC deposition number	2382749	2382750

[a] The data marked with "a" letter have been acquired through the Rietveld refinement of powder XRD patterns at RT.

hypothesize that as the temperature increases, the alpha-phase crystallohydrate likely transforms into the beta-phase, an orthorhombic ($C222_1$) $Zn_{2.5}$DOBDC structure, due to water loss and the incorporation of additional Zn^{2+} ions. The Zn-MOF-74a phase, on the other hand, was found to possess a trigonal unit cell ($R3c$) with a composition of Zn_2DOBDC·1.5H_2O.

Zn-MOF-74a

The overall structure of Zn-MOF-74a is very similar to the structure of regular MOF-74; however, here, each DOBDC molecule interconnects six Zn ions, forming a heart-like pore shape, which differs from the correct hexagonal shape observed in the classic MOF-74 structure (Tables S1 and S2†). The unit cell parameters are as follows: a = 22.9363(5) Å, c = 15.9389(3) Å. Refinement using a solvent mask confirmed the presence of 1.5 water molecules in pores per formula unit. The structure's steric accessibility, particularly at the octahedral Zn site in Zn-MOF-74a, suggests a higher likelihood of coordination with larger solvent molecules than MOF-74. This accessibility and the unique pore shape could offer potential advantages for specific applications, especially those involving larger molecules.

The asymmetric unit comprises two edge-sharing Zn crystallographic positions forming dimers and one DOBDC molecule. These Zn dimers are interconnected *via* DOBDC molecules. In contrast to the classic MOF-74, where metal sites are located at the junctions of three hexagonal pores and assembled into infinite edge-sharing chains, Zn-MOF-74a features metal sites along the walls connecting two pores, with no metal present at the junction points (Fig. 3). One Zn

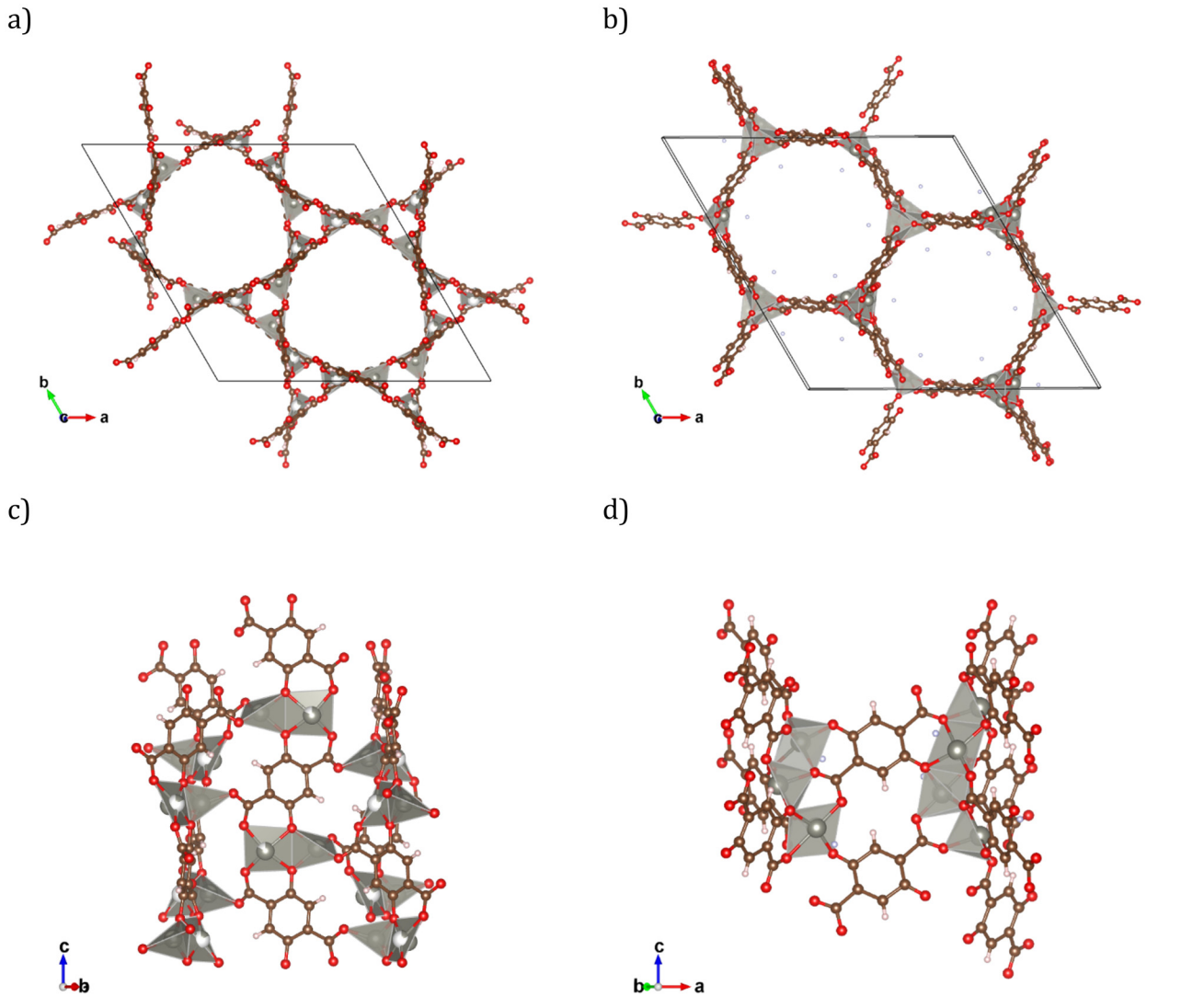

Fig. 3 Comparative structural analysis of MOF-74a and MOF-74. The projections along the c-axis reveal the distinct pore geometries: (a) heart-shaped pores in MOF-74a and (b) regular hexagonal pores in MOF-74. The wall sections between pores illustrate the arrangement of metal sites and DOBDC molecules: (c) in MOF-74a, where DOBDC molecules interconnect Zn_2O_8 dimers, and (d) in MOF-74, where the DOBDC molecules interconnect infinite chains of octahedral metal sites.

site is situated in a slightly distorted tetrahedral coordination environment (ZnO_4), with an average Zn–O bond length of approximately 1.94 Å. The second Zn site is split in a square planar configuration with a distance between the split sites about 0.53 Å. This configuration can be considered octahedral, where equatorial oxygens originate from the DOBDC molecule, and axial oxygens come from solvent molecules within the pores. The Zn–O bonds at this site have a slightly longer length of about 2 Å, consistent with octahedral coordination.

Due to the significant presence of solvent within the pores of the MOF structure, we could not conduct a Rietveld refinement to verify the accuracy of the calculated structural model for Zn-MOF-74a in bulk powder form (Fig. 4). Instead, we performed a Le Bail fitting, which confirmed the absence of any noticeable impurities in the sample. However, it is essential to note that the peak shapes exhibited apparent broadening, affecting the quality of the refinement, likely caused by texturing and microstrain resulting from variations in the solvent within the framework's pores.

Infrared spectroscopy was conducted to identify and compare the functional groups in MOF-74 and MOF-74a (Fig. S5†). Both spectra exhibit strong bands corresponding to the asymmetric stretching vibrations of the carboxylate groups' C═O bonds in the organic ligand, with maxima at 1551 cm^{-1} for MOF-74 and 1549 cm^{-1} for MOF-74a. Symmetric stretching vibrations of these groups are represented by absorption bands at 1364 cm^{-1} for MOF-74 and 1374 cm^{-1} for MOF-74a, with partial overlap from the intense C═C stretching band of the aromatic ring at 1421 cm^{-1}. Additionally, the MOF-74 spectrum displays C═C stretching bands at 1449 cm^{-1} and 1418 cm^{-1}. Weak absorption peaks at 1256 cm^{-1} and 1242 cm^{-1} are attributed to the stretching vibrations of phenolic C–O bonds. In the MOF-74a spectrum, a band at 1207 cm^{-1}, related to C–H β-stretching, also appears in MOF-74a with a maximum at 1193 cm^{-1}. Deformation vibrations of the C–H bonds in the benzene ring for MOF-74a are observed at 900 cm^{-1} and 828 cm^{-1}, while MOF-74 shows similar peaks at 886 cm^{-1} and 813 cm^{-1}.

The differences in Zn atom coordination between the structures are evident from the peaks corresponding to the Zn–O bond: the MOF-74 spectrum displays a low-intensity peak at 629 cm^{-1}, whereas the MOF-74a spectrum features an intense, bifurcated signal with peaks at 632 cm^{-1} and 605 cm^{-1} apparently related to different Zn coordination in the structures.

Broad bands in the 3600–2800 cm^{-1} region indicate the presence of trace water in the pores of both materials. In MOF-74a, this band likely results from water absorption from $Zn(CH_3COOH)_2{\cdot}2H_2O$. At the same time, the MOF-74 spectrum also includes a band at 1126 cm^{-1}, corresponding to C–O stretching in the methanol molecule, suggesting its possible presence in the pores. We found no evidence of THF presence in the MOF-74a sample.

To gain deeper insights into the samples' thermal stability and solvent content, TGA was performed on both MOF-74 and MOF-74a under air with a temperature ramp-up to 600 °C. The resulting mass-loss curves for both samples exhibited a similar profile, characterized by three distinct mass-loss events (Fig. 5).

The first mass-loss event occurred around 100 °C, predominantly due to the release of surface water. It is also hypothesized that this event includes water loss from the structural pores. MOF-74a exhibited nearly 50% more mass loss than MOF-74 up to this temperature, indicating a significantly higher water content and residual solvents within its pores. This discrepancy may be attributed to the distinct solvent retention properties of the two samples, as indicated by infrared spectroscopy: MOF-74 retains methanol, whereas MOF-74a lacks THF, which was used during its synthesis. The smaller size of water molecules compared to methanol could explain the relatively more straightforward release of solvents from the pores of MOF-74a.

The second mass-loss event, observed around 270 °C, corresponds to the evaporation of residual solvents from the pores of both samples. This stage marks the removal of any remaining volatile substances trapped within the frameworks. The presence of solvents is crucial for

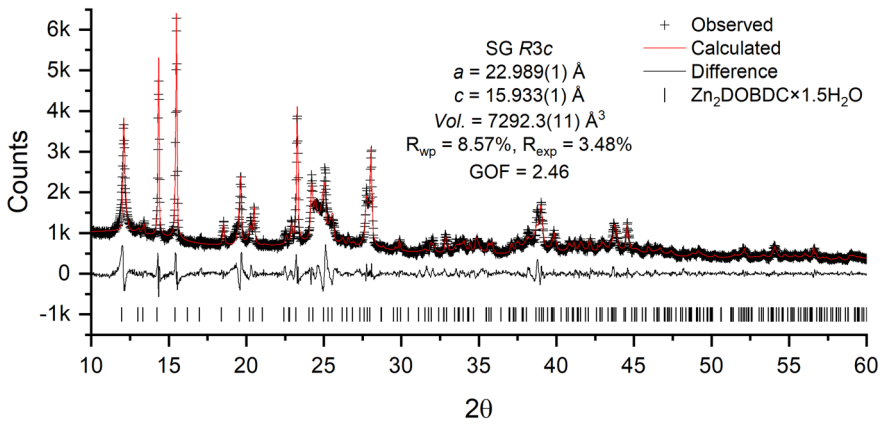

Fig. 4 Observed, calculated, and difference plot of Le Bail fitting on the X-ray diffraction data of Zn-MOF-74a $Zn_2DOBDC{\cdot}1.5H_2O$ (SG – *R*3*c*).

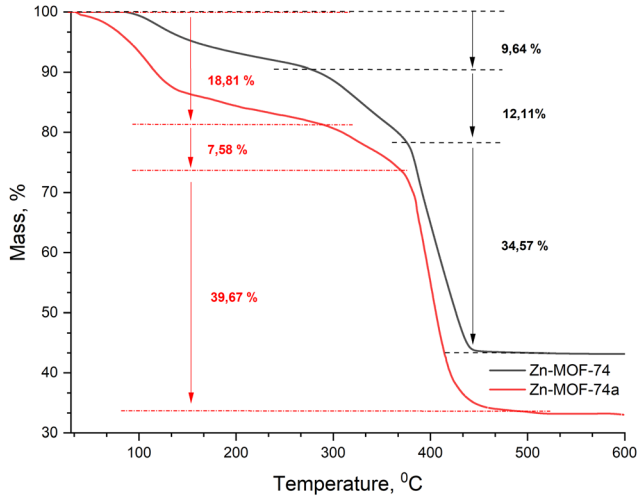

Fig. 5 TGA curves of MOF-74 and MOF-74a highlighting mass loss events and thermal decomposition profiles.

completing the coordination of Zn ions; hence, their removal leads to a significant decrease in structural stability.

The final significant mass-loss event occurred at approximately 380 °C, corresponding to the decomposition of the framework structures into ZnO. MOF-74 demonstrated slightly higher thermal stability, with decomposition initiating about 9 °C later than in MOF-74a. This difference in thermal behavior could be attributed to the local coordination environment of the Zn ions. In MOF-74, complete solvent removal leads to a square pyramid coordination of the Zn sites, whereas in MOF-74a, half of the Zn positions transit to a less stable square coordination. The square coordination is unfavorable and likely collapses into a tetrahedral coordination. This thereby destroys the framework.

Beta phase

While the indexing of the beta phase appears to align well with the orthorhombic ($C222_1$) unit cell, characterized by distinct cell parameters a = 28.161(2) Å, b 3.2672(2) Å, c = 9.075(7) Å, Vol. = 835.0(1) Å^3 (Fig. 6), our attempts to solve the structure using simulated annealing or charge flipping techniques on the powder diffraction pattern proved unsuccessful. Moreover, our endeavors to obtain a sufficiently large single crystal proved unfruitful. Although we acquired crystal-like particles of a size suitable for laboratory single-crystal X-ray diffraction, initial scans revealed these to be merely polycrystalline agglomerates. Surprisingly, despite a rather pronounced PXRD pattern following 2.5 days of the reaction, we encountered difficulties growing larger single crystals even after two weeks of synthesis.

To comprehensively investigate the composition of the beta phase, our study employed a combined TGA-MS approach, allowing us to analyze the evolving gaseous phases concurrently. This analysis was conducted under two distinct atmospheres: oxygen (O_2) and argon (Ar).

Specifically focusing on the beta phase within an O_2 atmosphere, our TGA-MS analysis revealed a distinct, single mass loss event, as depicted in Fig. 7. This characteristic mass loss can be attributed to the decomposition of the organic linker and commences at a temperature of 367.5 °C. The process concludes at 554 °C, with the complete conversion of the remaining ZnO. An initial 1.5% mass loss, seemingly associated with removing surface water, commenced at about 110 °C. Furthermore, the broad peaks observed in the mass spectrometry (MS) curves at m/z 44 (CO_2) and 18 (H_2O) are in harmony with the mass loss pattern associated with the combustion process.

What's intriguing is that the total observed mass loss stands at 42.62%, significantly deviating from the anticipated values of 49.79% for Zn_2DOBDC or 68.73% for ZnDOBDC. We suspected this deviation could be attributed to additional crystal water or solvent molecules within the structure. We repeated the experiment to eliminate a possible error and received the same result.

To investigate this, we conducted TGA-MS in a dry Ar atmosphere, where the sole potential water sources would be

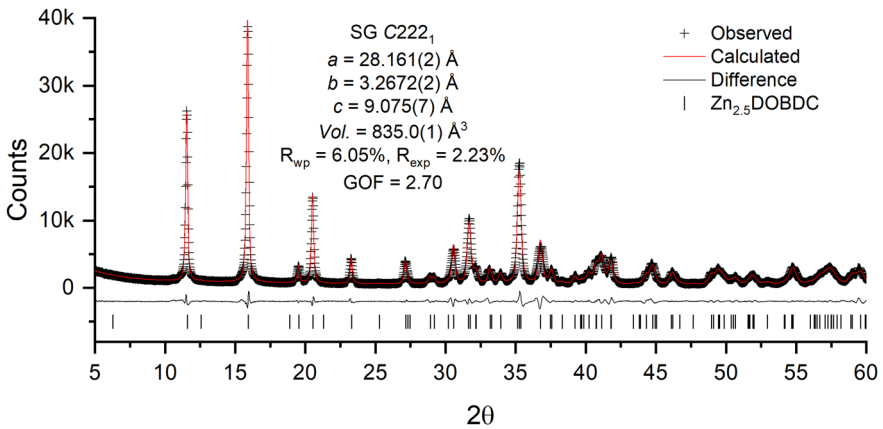

Fig. 6 Observed, calculated, and difference plot of Le Bail fitting on the X-ray diffraction data of beta phase $Zn_{2.5}$DOBDC (SG – $C222_1$).

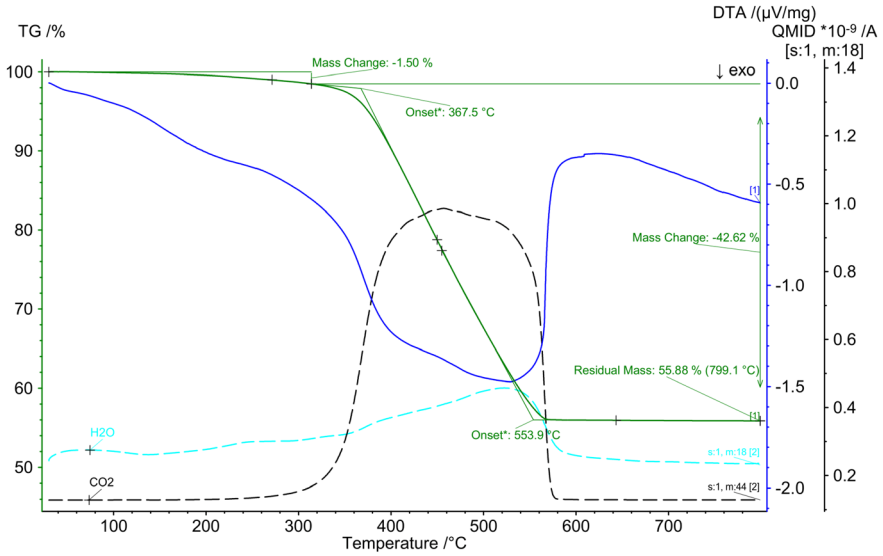

Fig. 7 Thermal gravimetric analysis coupled with mass spectrometry of the beta phase $Zn_{2.5}$DOBDC in an oxygen atmosphere. The green line illustrates the TG curve, the blue line represents the DTA curve, and the light blue, black, and red dashed lines depict the mass signals corresponding to H_2O, CO_2, respectively.

the products of material decomposition or crystalline water (Fig. 8). Any traces of THF incorporated into the structure would also be discernible in the mass-spec graph. Surprisingly, no significant mass loss events were detected before the primary material decomposition. As expected, the decomposition temperature of the beta phase in Ar was higher (529.5 °C), indicating increased stability in an inert medium. Additionally, we found no substantial amounts of water or traces of THF in the exhaust gases. The slight increase in the CO_2 m/z 44 curve after 250 °C could be attributed to the beginning of the gradual material decomposition, which peaks at 529.5 °C. Notably, benzene was the most significant organic compound detected, a direct product of the DOBDC organic linker decay. These observations, coupled with the findings from the O_2 experiment, strongly suggest the absence of structural water or solvent in the beta phase's crystal structure.

Given that the beta phase comprises solely Zn ions and DOBDC molecules, after meticulously considering the residual ZnO mass, we have deduced that the most plausible

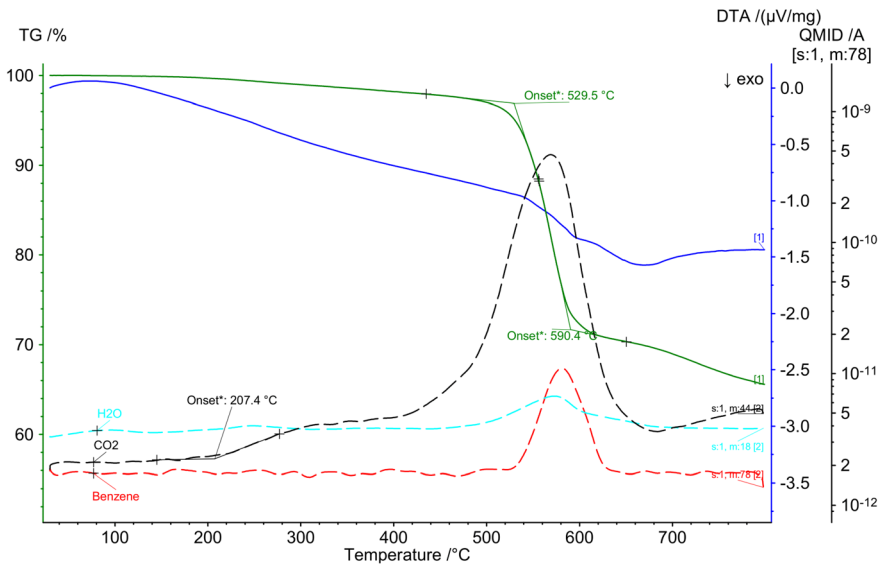

Fig. 8 Thermal gravimetric analysis coupled with mass spectrometry of the beta phase $Zn_{2.5}$DOBDC in an argon atmosphere. The green line illustrates the TG curve, the blue line represents the DTA curve, and the light blue, black, and red dashed lines depict the mass signals corresponding to H_2O, CO_2, and benzene, respectively.

explanation for this mass loss is the composition $Zn_{2.5}$-DOBDC. In this scenario, the total mass loss would account for 43.08%, closely aligning with the observed 42.62%.

The obtained composition $Zn_{2.5}$DOBDC is inherently intriguing due to the inherent characteristics of DOBDC, where the maximum oxidation state is −4, and $Zn_{2.5}$ is supposed to achieve a total oxidation state of +5. This seeming disparity might imply the presence of Zn^+ ions in the structure, which are typically unstable when existing as individual ions. However, the experimental evidence supports the stability of Zn–Zn dimers with a total oxidation state of +2, even under standard lab conditions.[31] Further confirmation of this is the saturated reddish color observed in the obtained beta phase, which is highly unusual for Zn^{2+} compounds.

Considering this, we propose a structural model where Zn ions can be differentiated based on the following scheme: Zn^{2+} + $1/2Zn^{2+}$ + Zn^+. This scheme results in the total +4 oxidation stage for 2.5 Zn ions while obeying the charge balance. In this configuration, Zn^+ ions might form dimers with other symmetrical Zn^+ ions, presumably located in adjacent unit cells. One Zn^{2+} ion occupies a general position, while the further halved Zn^{2+} ion occupies a special position with halved multiplicity. Such an arrangement is permissible within the $C222_1$ unit cell, with general positions having a multiplicity of 8 (Wyckoff position 8c) and special positions having a multiplicity of 4 (Wyckoff position 4b or 4a). This arrangement not only explains the observed composition of $Zn_{2.5}$DOBDC but also supports the accuracy of the chosen unit cell.

To confirm the stability and composition of the organic linker, we have examined the IR spectrum of the obtained beta phase (Fig. S5†). The spectral pattern of the beta phase of $Zn_{2.5}$DOBDC closely resembles that of the alpha phase, with one notable exception: the appearance of a distinct peak at 3500 cm^{-1}. This peak is supposed to be attributed to the remaining hydroxyl group in DOBDC. The absence of the broad absorption band in the 3500–2600 cm^{-1} range indicates the absence of Zn to water or OH bonds, confirming the absence of crystalline water, as indicated by TGA.[32,33]

Moreover, subtle shifts in peak positions in the region below 1600 cm^{-1} are observed, reflecting variations in the strength of metal–ligand bonds and the degree of delocalization of vibrational modes. Within the range of 1600–1500 cm^{-1}, specifically at 1536 cm^{-1}, the bands are identified as the carbonyl stretching vibrations of the carboxylate groups in the MOF ligand. Peaks in the vicinity of 1400 cm^{-1} are associated with the aromatic C=C groups, spanning from 1462 to 1370 cm^{-1}. Furthermore, the C–O and C–C stretching vibrations of the DOBDC ligand are manifested in the 1300–1000 cm^{-1} region, ranging from 1258 to 1123 cm^{-1}. Bands below 1000 cm^{-1} correspond to C–H vibrations, notably at 895 cm^{-1}, and Zn–O vibrations, spanning from 800 to 753 cm^{-1}.

Remarkably, any remaining protonated hydroxyl groups within the structure hint at the possibility of the DODBC ligand carrying a total charge lower than −4. Should the ligand's charge be −3 (indicating only one deprotonated hydroxyl group), we enter a structural scenario where Zn ions can be distinguished according to the following scheme: $1/2Zn^{2+}$ + $2Zn^+$. In this scenario, the $(Zn_2)^{2+}$ dimer forms within a single unit cell, with Zn^+ occupying a general position and Zn^{2+} in a special position.

However, should both hydroxyls of DOBDC remain protonated, the ligand's total charge is reduced to −2. In this situation, the Zn model implies the presence of Zn^0 in the system, a highly improbable scenario.

This discussion remains enigmatic, as both cases appear unusual and raise questions about their credibility. Further investigation of the crystal structure is imperative to provide a more comprehensive and precise understanding of the beta phase.

H_4DOBDC precursor

During our work, we found that though the organic linker precursor is commercially available, there has yet to be a published dry H_4DOBDC structure (H_4 is due to considering deprotonation of hydroxyl groups). Therefore, we encountered difficulties in the identification of the product compounds.

To address this issue, we have collected the powder XRD data on the dry H_4DOBDC and attempted to index it. The diffraction pattern was successfully indexed in the triclinic unit cell $P\bar{1}$ (Fig. 9). We assumed the determined molecule shape to solve the structure and added it as a rigid body. Since the lab powder XRD is very insensitive to hydrogen and H can rotate around the C–O bond, the rigid body did not include hydrogen of hydroxyl groups. The COO groups were allowed to rotate. The structure solution process was carried out using a simulated annealing method. Additionally, we suggested that the sample exhibits texturing and anisotropic broadening, resulting from the transition from the crystallohydrate to the anhydrous form.

The derived structural model revealed the formation of layered structures comprised of planar H_4DOBDC molecules interconnected *via* hydrogen bonding. These layers exhibited an inter-layer distance of approximately ~2.8 Å. The COO groups exhibited a slight rotation of approximately 10° relative to the benzene ring. The presence of this relatively low-symmetry unit cell can be ascribed to the intricate electrostatic interactions inherent to the molecule. Notably, we selected the $P\bar{1}$ space group, a choice that is not uncommon in the area of organic crystal structures. This selection was made while considering the constraints of our laboratory XRD equipment when dealing with structures of lower symmetry. Consequently, atomic positions were refined only with the rigid body approach. Comprehensive structural parameters can be found in Tables S5 and S6.†

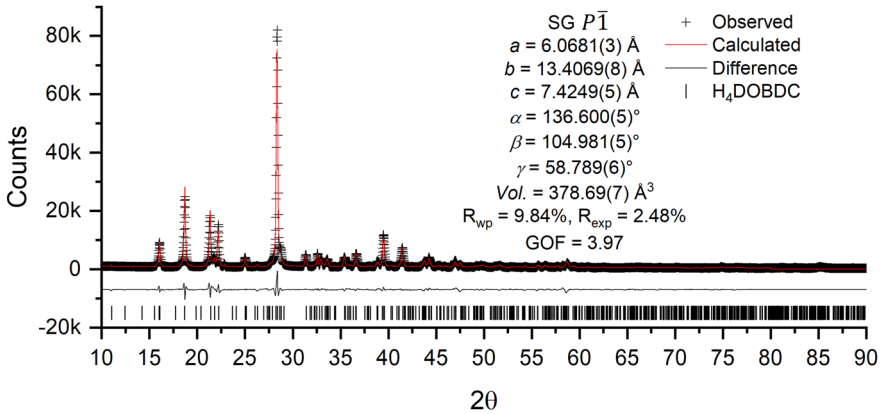

Fig. 9 Observed, calculated, and difference plot of Rietveld refinement on the X-ray diffraction data of alpha phase H_4DOBDC (SG – $P\bar{1}$).

A broad peak at 3080 cm^{-1} was identified in the precursor's IR spectrum (Fig. S5†), indicating the presence of O–H and C–O stretching vibrations associated with carboxylic acid (COOH) groups.[34] Another sharp peak at 1641 cm^{-1} was attributed to the C═O stretching vibration of the carboxylic acid groups. Additionally, the range between 1480–1495 cm^{-1} represented C═C stretching vibrations of carboxylate (COO^-) groups, while the peak at 1424 cm^{-1} indicated C–C stretching vibrations. C–O stretching vibrations were evidenced by the peak at 1176 cm^{-1}, and C–H bending vibrations were observed around 800 cm^{-1}.

Conclusion

In conclusion, this study explored the synthesis of Zn–DOBDC-based MOFs using tetrahydrofuran (THF) as a solvent, leading to the unexpected formation of three distinct metal–organic phases: alpha, beta, and Zn-MOF-74a, rather than the anticipated Zn-MOF-74 structure. Our findings demonstrate the influence of solvent choice, temperature, and pH on phase formation, with the alpha phase dominant at lower temperatures and the beta phase emerging at higher temperatures. The novel Zn-MOF-74a phase exhibits a unique pore structure and crystallographic properties, distinct from the conventional MOF-74. The primary advantage of synthesizing MOF-74a using THF is that THF is more easily removed from the structural pores post or during synthesis. This results in the formation of smaller pores, which may offer improved performance in specific applications, such as gas adsorption or separation.

The structural analysis, including X-ray diffraction, IR spectroscopy, and TGA, revealed important insights into the coordination environments, solvent interactions, and thermal stability of the obtained phases. Our study also reports the first successful determination of the dry H_4DOBDC precursor structure, providing a valuable reference for future research. Further investigations are needed to fully understand the beta phase's structure and the electrochemical properties of Zn-MOF-74a, which could offer pathways for optimizing MOFs in energy-related applications.

Data availability

The datasets obtained and analyzed during the current study are available from the corresponding author upon reasonable request. This includes the raw data from X-ray diffraction (XRD) experiments, infrared (IR) spectroscopy, and thermogravimetric analysis (TGA). Crystallographic information files (CIFs) for the newly identified Zn-MOF-74a and related phases and the dry H4DOBDC precursor have been deposited with the CCDC. Any additional experimental data or ESI† related to this study is also available upon request.

Author contributions

A. A. S. – investigation, methodology, writing – original draft; M. D. S. – investigation, data curation; V. A. D. – investigation, data curation; K. A. L. – investigation, data curation; A. M. S. – data curation; A. A. M. – investigation, methodology, data curation; A. K. G. – writing – review & editing; I. A. T. – conceptualization, methodology, writing – original draft, writing – review & editing.

Conflicts of interest

There are no conflicts of interest to declare.

Acknowledgements

The authors thank the Ministry of Science and Higher Education of the Republic of Kazakhstan (project AP14871991 and BR21882200) for financial support. The authors also thank Nazarbayev University Core Facilities for providing instrumental support.

References

1 S. Sangeetha, G. Krishnamurthy, S. Foro and K. Raj, *J. Inorg. Organomet. Polym. Mater.*, 2020, **30**, 4792–4802.
2 J. Cai, C. Liu, S. Tao, Z. Cao, Z. Song, X. Xiao, W. Deng, H. Hou and X. Ji, *Coord. Chem. Rev.*, 2023, **479**, 214985.

3 T. Li, Y. Bai, Y. Wang, H. Xu and H. Jin, *Coord. Chem. Rev.*, 2020, **410**, 213221.
4 X. Li, F. Cheng, S. Zhang and J. Chen, *J. Power Sources*, 2006, **160**, 542–547.
5 G. DeCombarieu, M. Morcrette, F. Millange, N. Guillou, J. Cabana, C. P. Grey, I. Margiolaki, G. Férey and J. M. Tarascon, *Chem. Mater.*, 2009, **21**, 1602–1611.
6 L. S. Xie, G. Skorupskii and M. Dincă, *Chem. Rev.*, 2020, **120**, 8536–8580.
7 C. Li, L. Zhang, J. Chen, X. Li, J. Sun, J. Zhu, X. Wang and Y. Fu, *Nanoscale*, 2021, **13**, 485–509.
8 J. P. Zhu, X. H. Wang and X. X. Zuo, *R. Soc. Open Sci.*, 2019, **6**, 190634.
9 J. G. Flores, J. Aguilar-Pliego, N. Martin-Guaregua, I. A. Ibarra and M. Sanchez-Sanchez, *Catal. Today*, 2022, **394–396**, 295–303.
10 S. Li, X. Zhu, H. Yu, X. Wang, X. Liu, H. Yang, F. Li and Q. Zhou, *Environ. Res.*, 2021, **197**, 111054.
11 X. Zhang, Q. Zheng and H. He, *Microporous Mesoporous Mater.*, 2022, **336**, 111899.
12 S. Chen, X. Li, J. Duan, Y. Fu, Z. Wang, M. Zhu and N. Li, *Chem. Eng. J.*, 2021, **419**, 129653.
13 Q. Al-Naddaf, A. A. Rownaghi and F. Rezaei, *Chem. Eng. J.*, 2020, **384**, 123251.
14 D. Wang, W. Zhou, R. Zhang, X. Huang, J. Zeng, Y. Mao, C. Ding, J. Zhang, J. Liu and G. Wen, *J. Mater. Chem. A*, 2018, **6**, 2974–2983.
15 L. Hu and Q. Chen, *Nanoscale*, 2014, **6**, 1236–1257.
16 Z. Xie, W. Xu, X. Cui and Y. Wang, *ChemSusChem*, 2017, **10**, 1645–1663.
17 Z. Guo, F. Yang, R. Yang, L. Sun, Y. Li and J. Xu, *Sep. Purif. Technol.*, 2021, **274**, 118949.
18 P.-H. Hsu, C.-C. Chang, T.-H. Wang, P. K. Lam, M.-Y. Wei, C.-T. Chen, C.-Y. Chen, L.-Y. Chou and F.-K. Shieh, *ACS Appl. Mater. Interfaces*, 2021, **13**, 52014–52022.
19 T. Stolar, A. Prašnikar, V. Martinez, B. Karadeniz, A. Bjelić, G. Mali, T. Friščić, B. Likozar and K. Užarević, *ACS Appl. Mater. Interfaces*, 2021, **13**, 3070–3077.
20 K. Xue, Y. Si, S. Xie, J. Yang, Y. Mo, B. Long, W. Wei, P. Cao, H. Wei, H. Guan, E. G. Michaelis, G. Guo, Y. Yue and C. Shan, *Front. Chem.*, 2021, **9**, 647545.
21 S. Ploychompoo, Q. Liang, X. Zhou, C. Wei and H. Luo, *Phys. E*, 2021, **125**, 114377.
22 C. N. Zhang, Y. Li, H. L. Fan, C. Yang and M. M. Wu, *J. Inorg. Organomet. Polym. Mater.*, 2020, **30**, 486–493.
23 J. G. Flores, M. Díaz-García, I. A. Ibarra, J. Aguilar-Pliego and M. Sánchez-Sánchez, *J. Solid State Chem.*, 2021, **298**, 122151.
24 D. Britt, H. Furukawa, B. Wang, T. G. Glover and O. M. Yaghi, *Proc. Natl. Acad. Sci. U. S. A.*, 2009, **106**, 20637–20640.
25 P. D. C. Dietzel, B. Panella, M. Hirscher, R. Blom and H. Fjellvåg, *Chem. Commun.*, 2006, 959.
26 A. A. Coelho, *J. Appl. Crystallogr.*, 2018, **51**, 210–218.
27 N. Nijem, J.-F. Veyan, L. Kong, H. Wu, Y. Zhao, J. Li, D. C. Langreth and Y. J. Chabal, *J. Am. Chem. Soc.*, 2010, **132**, 14834–14848.
28 W. Zhou, H. Wu and T. Yildirim, *J. Am. Chem. Soc.*, 2008, **130**, 15268–15269.
29 N. L. Rosi, J. Kim, M. Eddaoudi, B. Chen, M. O'Keeffe and O. M. Yaghi, *J. Am. Chem. Soc.*, 2005, **127**, 1504–1518.
30 N. E. Ghermani, G. Morgant, J. D'Angelo, D. Desmaële, B. Fraisse, F. Bonhomme, E. Dichi and M. Sgahier, *Polyhedron*, 2007, **26**, 2880–2884.
31 H. Li, M. Eddaoudi, T. L. Groy and O. M. Yaghi, *J. Am. Chem. Soc.*, 1998, **120**, 8571–8572.
32 R. Madhu, S. S. Sankar, K. Karthick, A. Karmakar, S. Kumaravel and S. Kundu, *Inorg. Chem.*, 2021, **60**, 9899–9911.
33 J.-J. Song, B. He, X. Wang, Y. Guo, C. Peng, Y. Wang, Z. Su and Q. Hao, *J. Mater. Sci.*, 2021, **56**, 17178–17190.
34 L. S. Flores, S. P. Alcântara, G. C. G. de Lima, M. I. Yoshida and C. C. Corrêa, *Vib. Spectrosc.*, 2016, **86**, 302–310.